

Baroclinic Multiple Zonal Jets on the Sphere

SUKYOUNG LEE

Department of Meteorology, The Pennsylvania State University, University Park, Pennsylvania

(Manuscript received 29 July 2004, in final form 5 December 2004)

ABSTRACT

Multiple zonal jets are investigated with a two-level primitive equation model on the sphere in which both baroclinicity and planetary radius are varied. As in the case for a two-layer quasigeostrophic model on a β -plane channel, it is found both that the Rhines scale successfully predicts the meridional scale of the multiple zonal jets, and that these jets are maintained in part by an eddy momentum flux divergence associated with slow baroclinic waves at the interjet minimum.

A scaling analysis suggests that $n_{\text{jets}} \propto (a/\theta_m)^{1/2}$, with the constraints $\zeta_e \equiv 8 \sin^2 f (\theta_m/\Delta\theta) > 1$ and $n_{\text{jets}} \geq 1$, where n_{jets} is the number of the jets, a the planetary radius, θ_m one-half of the pole-to-equator potential temperature difference, ξ_e the supercriticality of the two-layer Phillips model, $\Delta\theta$ the potential temperature difference between the two levels, and ϕ the latitude. The number of jets simulated by the model agrees with this scaling, provided that $L_{\text{jet}} \leq a$, where L_{jet} is the jet scale.

In model runs with a large planet where multiple zonal jets exist, the time-mean eddy heat flux is found to be consistent with the diffusive picture of Held and Larichev. In contrast, for the model runs with the planetary size equal to that of Earth, baroclinic adjustment is found to be more relevant. These results are consistent with the finding that in the large-planet (Earth-like) model runs, the jet/eddy scale is smaller than (comparable to) the corresponding planetary radius.

1. Introduction

The theory of β -plane turbulence (Rhines 1975, 1977) motivated the search for multiple jets in both barotropic (Williams 1978; Yoden and Yamada 1993; Huang and Robinson 1998; Huang et al. 2001) and shallow water (Cho and Polvani 1996) models. Multiple-jet states are also found in baroclinic flows where disturbances are spontaneously generated by baroclinic instability (Williams 1979; Panetta and Held 1988; Vallis and Maltrud 1993; Panetta 1993; Lee 1997).

Various scalings (Rhines 1975; Vallis and Maltrud 1993; Held and Larichev 1996) for β -plane turbulence yield values that are very similar to each other (Vallis and Maltrud 1993; Held 1999; Williams 2003), and are generally well supported by numerical simulations (Vallis and Maltrud 1993; Panetta 1993). Taking these fundamental results as given, Lee (1997) examined the maintenance mechanism for multiple baroclinic jets in a

quasigeostrophic (QG) β -plane channel. In this QG model, β is nondimensionalized by U/λ^2 with U being the equilibrium vertical shear and λ the Rossby radius of deformation. This nondimensional parameter is denoted as β^* . It was found that the multiple jets tend to be more persistent for high β^* and for the relatively low surface friction regime of this model. In that regime, it was shown that the multiple jets are maintained by eastward propagating, fast baroclinic waves that are absorbed at their critical latitudes, where the wave phase speed equals the local zonal wind speed. In addition, the jets are also shown to be maintained by an equatorward vorticity flux (i.e., meridional divergence of zonal momentum) at the local jet minima between the jets, carried out by slow, westward propagating baroclinic waves.

The primary goal of this study is to examine if the same multiple-jet maintenance mechanism can operate for Earth-like β^* , with a spherical geometry. Because the range of realistic values for U and λ is wide enough to encompass both the low- and high- β^* parameter regime, it is unclear a priori to what extent the above jet maintenance mechanism is representative for the atmosphere. Williams (2003) finds that persistent multiple

Corresponding author address: Suhyoung Lee, Dept. of Meteorology, 522 Walker Building, The Pennsylvania State University, University Park, PA 16802.
E-mail: sl@meteo.psu.edu

jets are also ubiquitous in a Jupiter-like atmosphere on the sphere with a thin baroclinic layer. Similar results are obtained in GCMs when the rotation rate of the Earth is increased by more than a factor of two (Williams 1988). Nonetheless, considering latitudinal asymmetries posed by the latitudinal variation of β (Williams 1988), and metric terms (Whitaker and Snyder 1993), it is also uncertain a priori whether the maintenance mechanism in the QG β -plane channel also operates in the primitive equation system on the sphere.

A secondary goal of this study is to gain better insight into equilibrium processes in the presence of the baroclinic eddies. One prominent view has been that the statistical equilibrium state corresponds to the marginal state for baroclinic instability, where the equilibrium process is referred to as baroclinic adjustment (Stone 1978). While there are a number of different ways for the marginal state to be achieved (e.g., Stone 1978; Lindzen et al. 1980; Cehelsky and Tung 1991; Gutowski 1985; Lindzen 1993; Nakamura 1999), and the relevance of some of these processes has been questioned (Thuburn and Craig 1997; Barry et al. 2000), in two-layer models with terrestrial parameter settings, the operation of baroclinic adjustment through the meridional mixing of the thermal field seems to be robust (Stone 1978; Cehelsky and Tung 1991; Stone and Branscome 1992). Even in the two-layer model, however, Pavan and Held (1996) show that the diffusive picture of Held and Larichev (1996) holds well, and that baroclinic adjustment is unlikely to operate unless the baroclinic zone is sufficiently narrow.¹ While these results are already insightful, once again, because a nondimensional β -plane channel model was used, it is still uncertain whether the width of Earth's baroclinic zone belongs to the narrow or wider diffusive regime. By comparing eddy fluxes from planets of two different sizes (see section 2 for the rationale behind the choice of the hypothetical planet size), this study addresses the relationship between the width of the baroclinic zone and the two equilibrium pictures—baroclinic adjustment and the diffusion—in a model whose result can be more readily interpreted.

Section 2 briefly describes the numerical model used in this study and explains the analysis approach. The main results concerning the multiple jets are described in sections 3 and 4, and section 5 addresses the baro-

clinic adjustment and diffusive pictures. The conclusions follow in section 6.

2. Model description and experimental design

a. Model

This study uses the two-level primitive equation model (e.g., see Held and Suarez 1978; Hendon and Hartmann 1985; Saravanan 1993; Lee and Held 1993). This global spectral model is written in pressure coordinates with finite differencing in the vertical. The horizontal velocity and potential temperature fields are calculated at 250 and 750 mb. The vertical velocity at the upper and lower boundaries, as well as the vertically averaged horizontal divergence, are set to zero. The potential temperature difference between the two levels, $\Delta\theta$, is set to 30 K, and the global mean temperature θ_o is fixed at 315 K.

The lower-level wind is subject to mechanical damping. Unless stated otherwise, the time scale for this damping is set at 10 days. This is a rather weak damping for the atmosphere, but it allows for the formation of strong eddy-driven jets. Model runs with a 5-day damping are also examined and it is found that the results are qualitatively similar to the runs with the 10-day damping. The horizontal winds and potential temperature are subject to biharmonic horizontal diffusion. The value of the diffusion coefficient is $1 \times 10^{17} \text{ m}^4 \text{ s}^{-1}$. Because this two-level model is prone to equatorial superrotation (Saravanan 1993), interfacial friction between the two levels is also included to avoid such a state. The required minimum value for this interfacial friction becomes greater as the horizontal resolution decreases and the baroclinicity increases. For the horizontal resolution and the maximum value of baroclinicity used in this study, the case where θ_m in (1) is set equal to 80 K, it was found that 50-day interfacial damping time scale is necessary. As such, this value is used for all model runs shown in this study. Lastly, the vertically averaged potential temperature is relaxed toward a radiative-equilibrium state Θ_e , prescribed as

$$\Theta_e = \theta_o + \frac{2\theta_m}{3}(1 - 3\sin^2\phi), \quad (1)$$

where ϕ is the latitude, θ_o is the global mean potential temperature, and $2\theta_m$ is the potential temperature difference between the equator and the pole. The radiative relaxation time scale is fixed at 30 days.

b. Choice of a large planetary size

By definition, multiple zonal jets can exist only if the domain size is much greater than the jet scale. If these

¹ In this theory, the eddy fluxes play a role that is similar to molecular diffusion in the sense that the eddy fluxes are determined by the local properties of the mean state. In contrast, for baroclinic adjustment, the eddy fluxes are determined by the global properties of the mean state.

jets are driven by eddies, it follows that meridional scale of the eddies must also be sufficiently smaller than the domain size. Taking the Earth's atmosphere as a reference state, there are a number of different ways to achieve such a state. For example, by increasing the rotation rate, and thereby decreasing the Rossby deformation radius, λ , Williams (1988) obtained multiple zonal jets in the extratropics.

Alternatively, the size of the planet may simply be increased to generate multiple jets. We chose to take this alternative approach because the value of λ is independent of the planetary radius. This property has two advantages. First, it eliminates the need for having to increase the model resolution. Of course, an increase in the planetary size requires a proportional increase in the total wavenumber in the model. However, because the physical grid size does not change, provided that the root-mean-square (rms) velocity of the eddies is fixed [see (3) below], the number of time steps required for computational stability still remains the same. Second, keeping λ constant simplifies the interpretation of the results to be presented in section 5.

With the above motivation we now ask, what is the minimum radius of a planet, a_L , for which more than one eddy-driven jet can fit into either hemisphere?² To determine the value for a_L , the following scaling analysis is considered. As shown by Panetta (1993), it is first assumed that the meridional scale of the energy-containing eddies and jets in a baroclinic flow is the Rhines scale [Vallis and Maltrud (1993) considered two other scales at which the inverse energy cascade halts, and showed that all three scales are qualitatively similar],

$$L_\beta = \left(\frac{u_{\text{rms}}}{\beta} \right)^{1/2} = a^{1/2} \left(\frac{u_{\text{rms}}}{2\Omega \cos\phi} \right)^{1/2}, \quad (2)$$

where u_{rms} is the rms velocity of the eddies, which is defined as the deviation from the zonal mean. All other symbols are standard. If it is further assumed that u_{rms} is proportional to the baroclinicity of the radiative equilibrium state, taking the supercriticality ξ_e of the Phillips two-layer model (Phillips 1956) as a measure for the baroclinicity, one may write

$$u_{\text{rms}} \propto \xi_e = 8 \sin^2\phi \frac{\theta_m}{\Delta\theta}, \quad (3)$$

² It needs to be noted that while a double jet state exists in the atmosphere (e.g., Southern Hemisphere equinoctial conditions), one of these jets is a subtropical jet that is driven by a thermally direct, overturning Hadley circulation (e.g., Krishnamurti 1961; Palmen and Newton 1969; Lee and Kim 2003), not by the eddies.

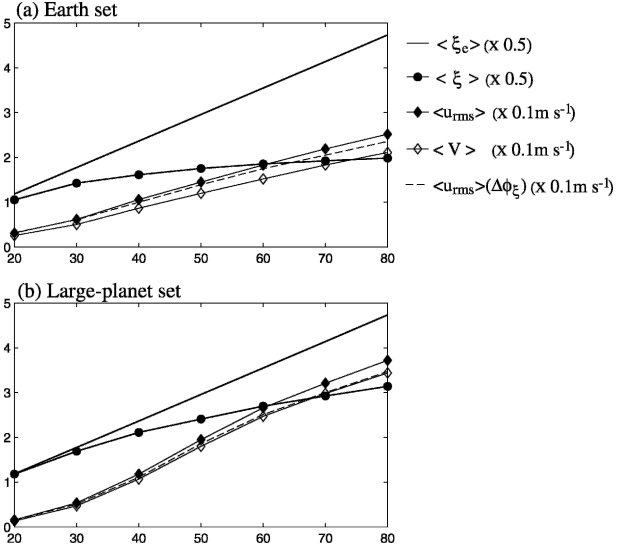


FIG. 1. Latitudinal average (from 22.5° to 67.5°) of supercriticality of the equilibrium state, $\langle \xi_e \rangle$ (solid line), supercriticality of the statistically steady state, $\langle \xi \rangle$ (filled circles), rms total velocity (filled diamonds) $\langle u_{\text{rms}} \rangle$, and rms barotropic velocity (open diamonds) $\langle V \rangle$ for (a) the Earth and (b) the large-planet set. Also shown is an alternative rms total velocity (dashed line), where the averaging is taken from ϕ_ξ to $\phi_\xi + 60^\circ$.

provided that $\xi_e > 1$, that is, that the radiative equilibrium state satisfies the Charney–Stern necessary condition for baroclinic instability (Charney and Stern 1962).³ The equality in (3) stems from (1), a special form for the equilibrium temperature profile. See the appendix for a derivation of ξ_e corresponding to the primitive equation (PE) model used in this study. In the numerical results shown in Fig. 1, which will be revisited later, there is indeed a linear relationship between $\langle \xi_e \rangle$ and $\langle u_{\text{rms}} \rangle$, where $\langle \cdot \rangle$ denotes an area-weighted latitudinal average extending from ϕ_S to ϕ_N :

$$\langle A \rangle \equiv \frac{\int_{\phi_S}^{\phi_N} A \cos\phi d\phi}{\int_{\phi_S}^{\phi_N} \cos\phi d\phi}.$$

³ This assumption is based on the fact that u_{rms} ultimately arises from baroclinic instability, and is motivated by our desire to express u_{rms} in terms of an externally imposed baroclinicity. As such, the assumption is not based on any particular turbulence theory. However, it needs to be noted that there is a resemblance between our assumption [see (3) below] and the result of Held and Larichev (1996) who based their scaling analysis on a homogeneous turbulence theory. They suggest the scaling $V = U\xi_e$, where U is the vertical wind shear, and V is rms barotropic velocity.

Unless stated otherwise, ϕ_S and ϕ_N are set equal to 22.5° and 67.5° , respectively. When this averaging is performed with the model output, the meridional grid points closest to ϕ_S and ϕ_N are chosen as the southern and northern limits. With the expression given by (A5), the value for $\langle \xi_e \rangle$ can be obtained analytically, and displayed in Fig. 1. The difference between this value and the one based on the model grid points, which is calculated numerically, is minimal (not shown). For each meridional grid, u_{rms} is set equal to the square root of the total eddy kinetic energy (EKE), averaged over time and longitude.

Neglecting the latitudinal variation, given $\Delta\theta$, (3) states that u_{rms} and ξ_e depend only upon the equator-to-pole temperature difference regardless of the planetary size. In other words, the baroclinicity is proportional to the equator-to-pole temperature difference $2\theta_m$, and not to the gradient. This is because of the factor of $1/a$ in β , which is in the denominator of ξ_e (see appendix).

According to (2) and (3), it is found that

$$L_\beta \propto \left(\frac{8 \sin^2 \phi / \Delta\theta}{2\Omega \cos \phi} \right)^{1/2} (a\theta_m)^{1/2}.$$

Again, neglecting the latitudinal variation, given Ω and $\Delta\theta$, the above relation reduces to $L_\beta \propto (a\theta_m)^{1/2}$. From this relation, and continuing to assume that the jet scale is determined by L_β , we can estimate the number of jets, n_{jets} , by a/L_β , which results in

$$n_{\text{jets}} \equiv a/L_\beta \propto (a/\theta_m)^{1/2}, \quad (4)$$

with the constraint $\xi_e > 1$ [the constraint for (3)] and $n_{\text{jets}} \geq 1$. The lowest latitude ϕ_ξ , beyond which the flow becomes supercritical ($\xi_e > 1$), is calculated from (A5) by solving for ϕ with $\xi_e = 1$. This latitude is indicated in Fig. 2. For all θ_m considered in this study, ϕ_ξ is in the Tropics/subtropics, ranging from 20.7° for $\theta_m = 30$ K to 12.5° for $\theta_m = 80$ K, indicating that a/L_β is a reasonable first-order estimate for n_{jets} .

For given θ_m , if one hemisphere of Earth is just broad enough for a single eddy-driven jet to fit, keeping everything else the same, (4) suggests that for two eddy-driven jets to fit within the domain, the required minimum radius of a_L is 4 times greater than Earth's radius. Likewise, if one hemisphere of Earth is broader than a single jet, but not quite broad enough for double jets, one may expect three eddy-driven jets in that quadrupled hypothetical planet. Guided by this estimate, two sets of model integrations are performed: for the first set, the radius of the planet is that of Earth (Earth set, hereafter); for the second set, the planetary radius is 4 times greater (large-planet set, hereafter) than

Earth's radius. The values for θ_o and static stability (see section 2a) are held fixed, and Ω is set equal to the value for Earth, which keeps λ constant throughout all model runs.

To hold the model resolution in these two sets constant, we chose to truncate at rhomboidal 15 (R15; Elsaesser 1966) for the Earth set, and at R60 for the large-planet sets. Although this resolution is rather low, previous studies suggest that this level of resolution is adequate for the present study, which is concerned only with the qualitative characteristics of the general circulation. As an example, for the equatorial superrotation examined by Saravanan (1993), a model truncated at triangular 21 (T21; Platzman 1960), which is similar to R15, yields results qualitatively similar to those produced by the same model truncated at T42.

For each set, seven runs are made, each with differing values of θ_m [see (1)]: 20, 30, 40, 50, 60, 70, and 80 K. The model statistics are calculated from the last 1000 days of a 1500 model day integration.

3. Jet structure dependency on a and θ_m

The time-mean zonally averaged upper- and lower-level zonal winds are shown in Fig. 2. The top row is for the Earth set, and the bottom two rows are for the large-planet sets. For each panel, the corresponding θ_m value is indicated in the bottom right corner. Consistent with the result of Stone and Branscome (1992), the $\theta_m = 20$ K case is close to a neutral state, as the eddy energy is very low (see Fig. 1). For this reason, the corresponding circulation is not shown.

As discussed in the section 2b, (4) suggests that there would be either two or three eddy-driven jets in the large-planet set. Figure 2 shows that this is indeed the case. For $\theta_m = 30$ K, there are three eddy-driven jets, centered at 35° and 55° , and a hint of a third jet at 70° (see also Fig. 3a). The fact that these jets are driven by eddy fluxes can be seen by the presence of lower-level westerlies (Fig. 2), the positive eddy momentum flux convergence (Figs. 2 and 8b), and the corresponding storm tracks indicated by EKE maxima (Fig. 3d). The jet centered close to 15° is a subtropical jet, as indicated by near zero values for both the lower-level zonal winds and the eddy momentum flux convergence (Fig. 2), an eastward Coriolis torque (not shown), and also by the absence of an associated storm track (Fig. 3d). Clearly such a jet is absent in the channel models (e.g., Vallis and Maltrud 1993; Panetta 1993).

In the corresponding Earth run, there is only a single jet with the upper-level jet being much wider than the

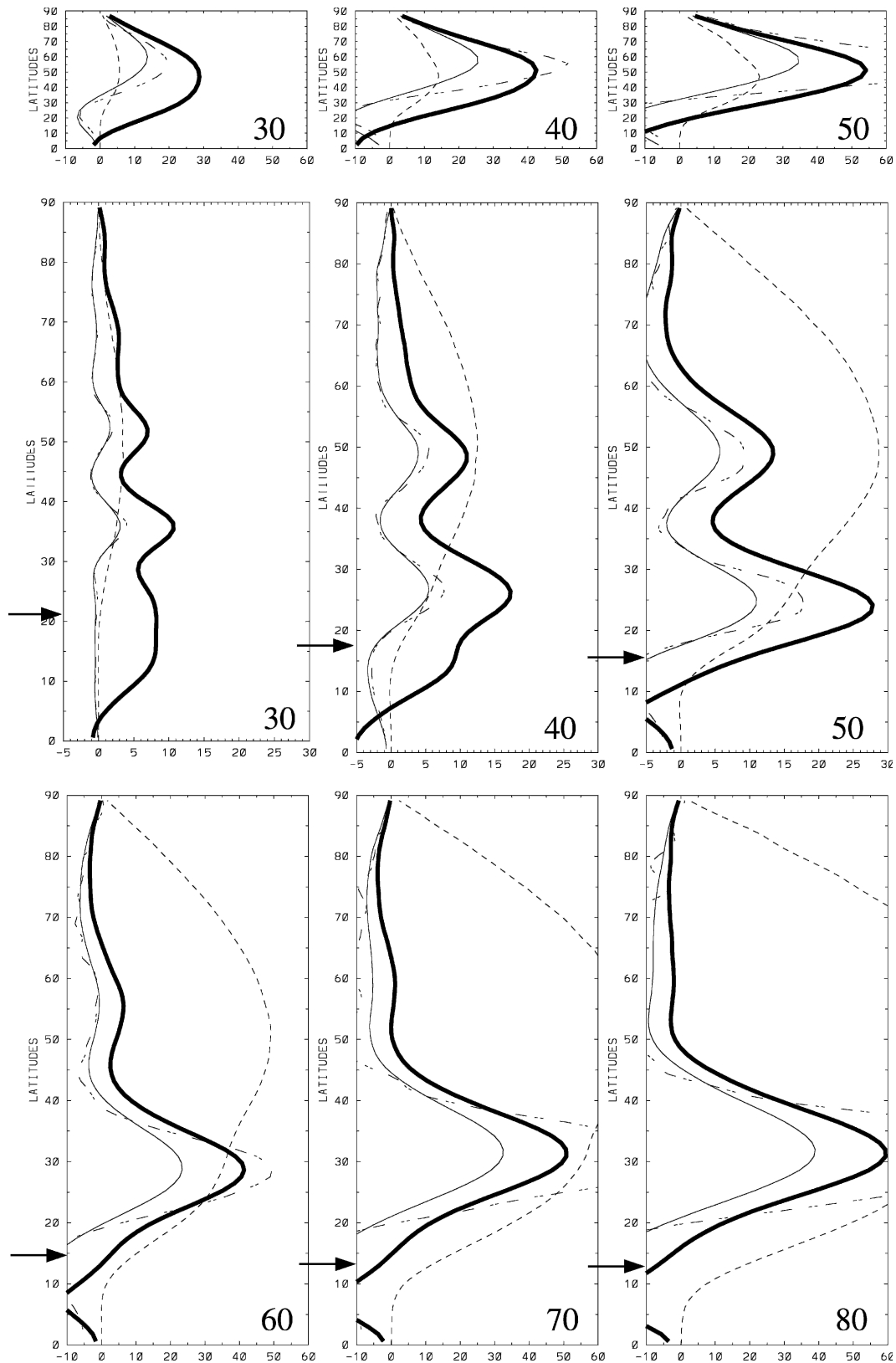


FIG. 2. Time- and zonal-mean zonal winds in the upper (thick solid line) and the lower (thin solid line) levels in m s^{-1} , upper-level eddy momentum flux convergence (long dashed line) in 10^{-6} m s^{-2} , and lower-level eddy heat flux (short dashed line) in $\text{m s}^{-1} \text{ K}$ for (top) the Earth set and (bottom) the large-planet set. The value for θ_m is indicated in the lower right corner of each panel. The arrows in the bottom two rows indicate ϕ_ξ . To avoid clutter, ϕ_ξ is not indicated for the Earth set.

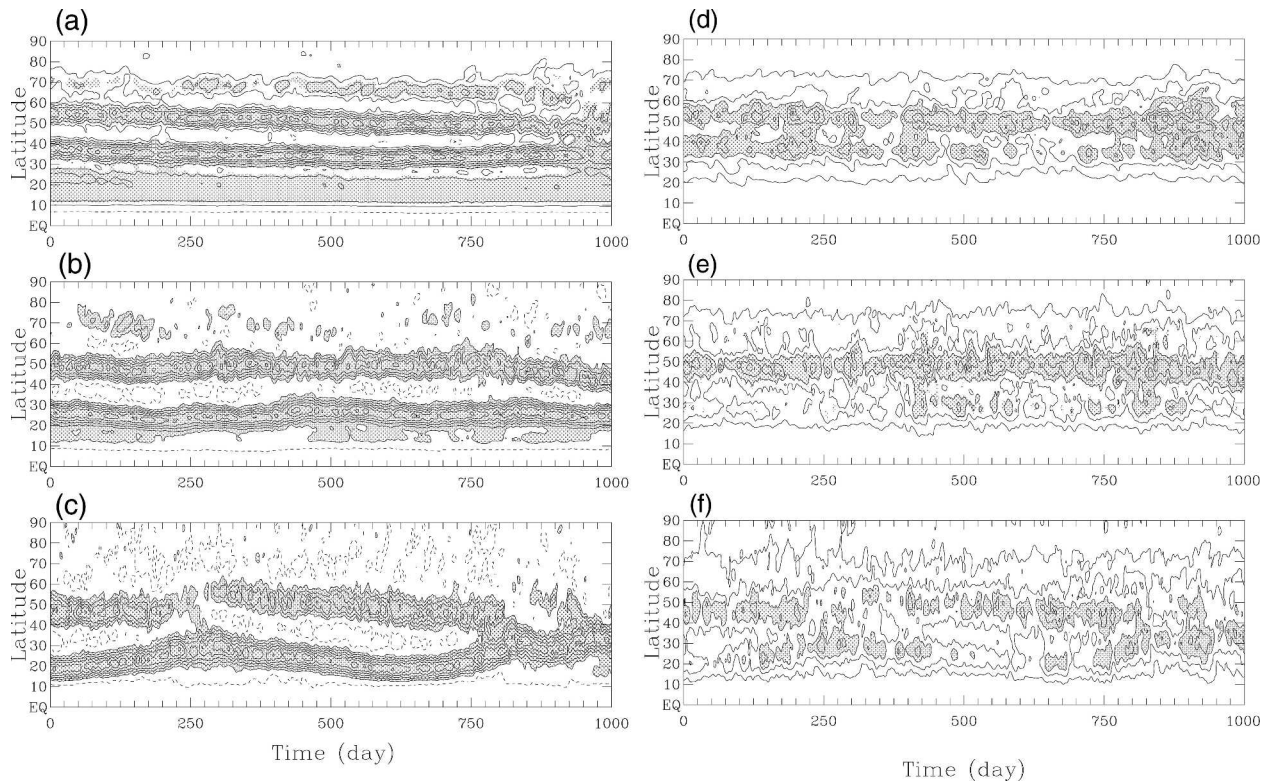


FIG. 3. Time series of anomalous zonal-mean zonal winds for (a) $\theta_m = 30$, (b) 40, and (c) 50 K in the large-planet set. The anomaly is the deviation from an arbitrary basic state, defined as $0.15 \times \theta_m \cos^2 \phi$ where ϕ is the latitude. This basic state is subtracted from the total field for display purposes. The contour interval is (a) 1.5, (b) 3.0, and (c) 5.0 m s^{-1} . The shading is above (a) 2.5, (b) 3.0, and (c) 5.5 m s^{-1} . (d), (e), and (f) The time series of EKE corresponding to (a), (b), and (c), respectively. The contour interval is (a) 1, (b) 50, and (c) 150 $\text{m}^2 \text{s}^{-2}$. The shading is above (a) 30, (b) 140, and (c) 450 $\text{m}^2 \text{s}^{-2}$.

lower-level westerlies.⁴ This lower-level westerly profile closely matches that of the eddy heat and vorticity fluxes both in position and in meridional extent, indicating that the eddy-driven portion of the jet is confined meridionally by the lower-level westerlies. Therefore, the fact that the upper-level jet is much broader than the lower-level westerlies implies that the single upper-level jet in this Earth run combines both the eddy-driven and the subtropical jets. A comparison with the corresponding large-planet run suggests that the blending of the two jets in the Earth run owes itself to the relatively small domain size. This same observation was also made by Williams and Holloway (1982) in their

numerical simulations in which the rotation rate of the planet is gradually varied.

For the large-planet run with $\theta_m = 40$ K (Fig. 2), there are two eddy-driven jets centered at 27° and 48°, with the former overlapping with the subtropical jet at 15°. At 70°, although there is no apparent evidence of a jet in the time-mean flow, a jet does form intermittently at this latitude (see Fig. 3b). As for the 30-K case, these jets are closely associated with EKE (Fig. 3e), and with eddy momentum flux convergence. Compared with the 30-K case, however, the jets now exhibit marked meridional meanders, reminiscent of the examples shown in Panetta (1993). In addition, the subtropical jet is no longer distinct, although a hint of it can be seen at $\approx 13^\circ$ in Fig. 2.

When θ_m is further increased to 50 K, there are still two eddy-driven jets (Fig. 2), but they occasionally merge (Fig. 3c). In addition, there is no evidence of a separate subtropical jet. With even larger values of θ_m (see the third row in Fig. 2), the flow is dominated by a single jet centered at 30°, and the maximum wind speed continues to increase.

⁴ In this study, a single jet is regarded as having one maximum, without discerning the presence of a separate subtropical jet. In previous studies with this type of two-level model and with a meridional temperature gradient of comparable strength, a hint of a subtropical jet can be seen in simulations that have both a higher horizontal resolution and stronger surface friction (Hendon and Hartmann 1985; Saravanan 1993). However, none of these simulations show two separate jet maxima.

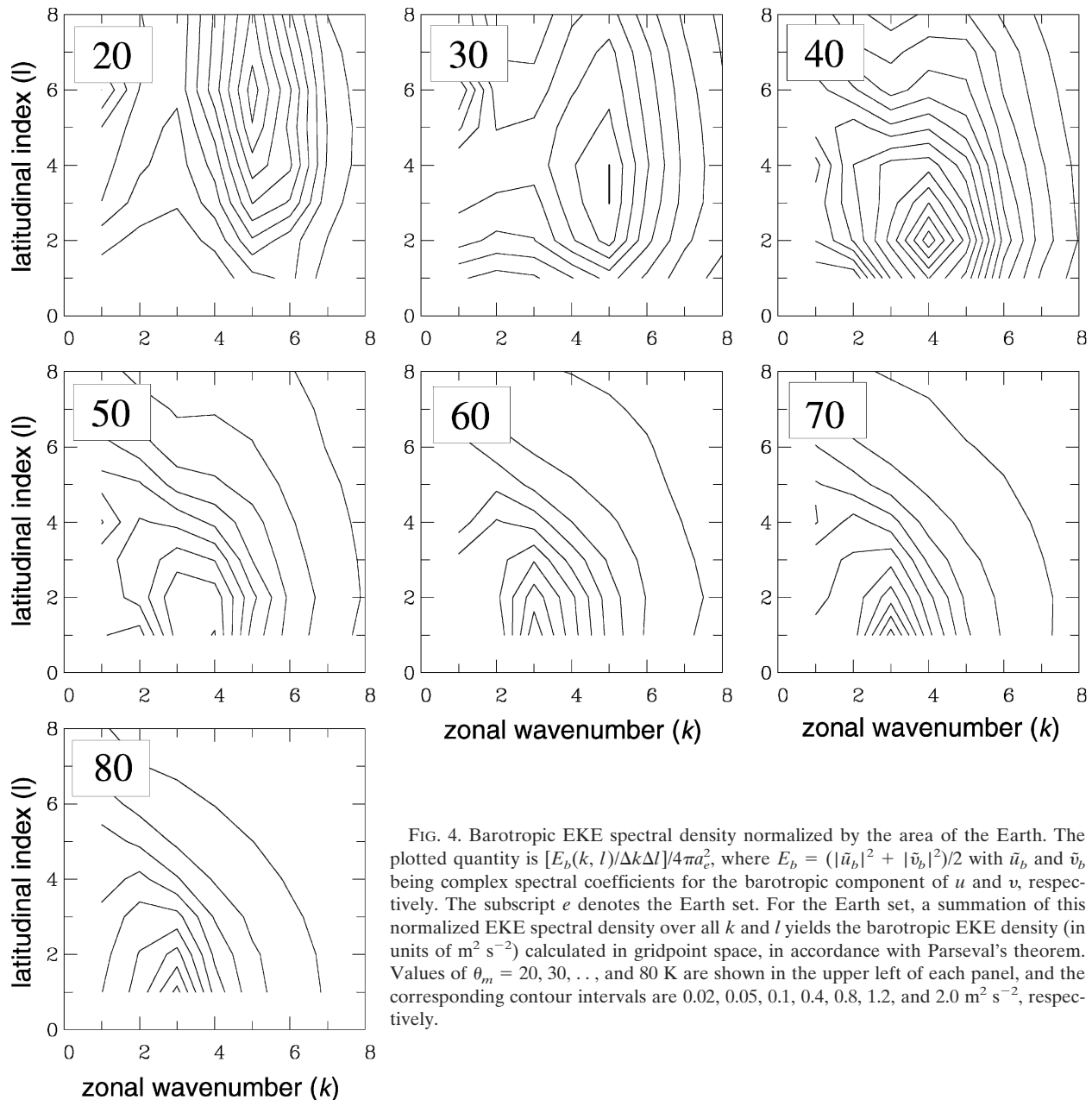


FIG. 4. Barotropic EKE spectral density normalized by the area of the Earth. The plotted quantity is $[E_b(k, l)/\Delta k \Delta l]/4\pi a_e^2$, where $E_b = (|\tilde{u}_b|^2 + |\tilde{v}_b|^2)/2$ with \tilde{u}_b and \tilde{v}_b being complex spectral coefficients for the barotropic component of u and v , respectively. The subscript e denotes the Earth set. For the Earth set, a summation of this normalized EKE spectral density over all k and l yields the barotropic EKE density (in units of $\text{m}^2 \text{s}^{-2}$) calculated in gridpoint space, in accordance with Parseval's theorem. Values of $\theta_m = 20, 30, \dots$, and 80 K are shown in the upper left of each panel, and the corresponding contour intervals are $0.02, 0.05, 0.1, 0.4, 0.8, 1.2$, and $2.0 \text{ m}^2 \text{ s}^{-2}$, respectively.

The above systematic decrease in n_{jets} for the large-planet set is directly linked to an equally systematic increase in the jet width. Similar systematic changes, however, do not take place in the Earth set (see Figs. 2a–c). As discussed above, and will be further explored below, this difference between the two sets is believed to be caused by the fact that the scale of the energy-containing eddies is limited by the size of the Earth.

Figures 4 and 5 show barotropic EKE spectral density for the Earth and large-planet sets, respectively. Note that the zonal kinetic energy is not displayed in

these figures. Following Baer (1972), the EKE spectral density from the spherical model is displayed as a function of k and the latitudinal index $n - k$, where k is the zonal wavenumber of the order, and n is the degree of the spherical harmonic. The latitudinal index $n - k$ is the number of zeros between the two poles. Noting that this latitudinal index is analogous to meridional wavenumber, for the sake of brevity, $n - k$ is denoted as l . As the supercriticality increases, there is an increasing amount of eddy energy accumulating at the smallest latitudinal index, implying that the finiteness of the

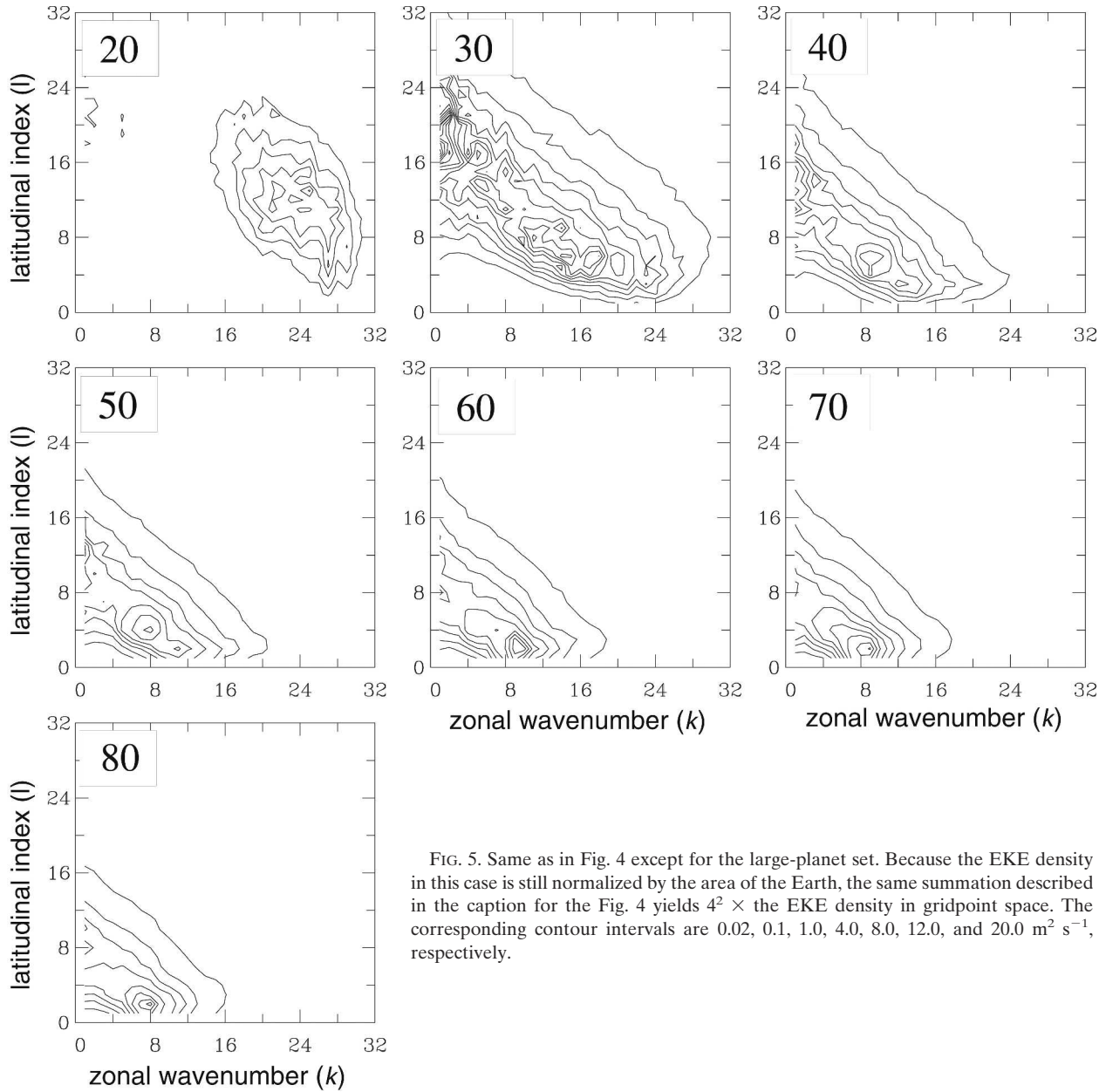


FIG. 5. Same as in Fig. 4 except for the large-planet set. Because the EKE density in this case is still normalized by the area of the Earth, the same summation described in the caption for the Fig. 4 yields $4^2 \times$ the EKE density in gridpoint space. The corresponding contour intervals are 0.02, 0.1, 1.0, 4.0, 8.0, 12.0, and 20.0 $\text{m}^2 \text{s}^{-1}$, respectively.

flow domain plays an increasingly important role. For the Earth set, this takes place at as small a value as 40 K, indicating that for this value of θ_m , which is regarded as a typical value for the atmosphere during the winter season, the upscale energy cascade is already limited by the domain size. For the large-planet set, the sign of energy accumulation at the smallest latitudinal index is evident only for the three most supercritical cases.

The results in Figs. 1, 4, and 5 suggest that above a certain value of θ_m , u_{rms} is limited by the domain size. This threshold value for θ_m appears to be somewhere near 40 K for the Earth set, and 60 K for the large-

planet set. If this is the case, the scaling (4), which is based on the Rhines scale, is expected to be valid only for the 30-K, and perhaps 40-K cases. Indeed, for these two cases, the jet widths in the large-planet set show the predicted twofold increase relative to the corresponding Earth set (see the dashed line in Fig. 6a).

Figure 6b shows an estimate of n_{jets} within the latitudinal range between ϕ_ξ and $\phi_\xi + 60^\circ$ (see section 2 for the definition of ϕ_ξ). The distance covered by this latitudinal range is $\pi a/3$. Thus, the estimate of n_{jets} was obtained by dividing this distance by L_β . For the calculation of L_β , we follow Panetta (1993) and once again

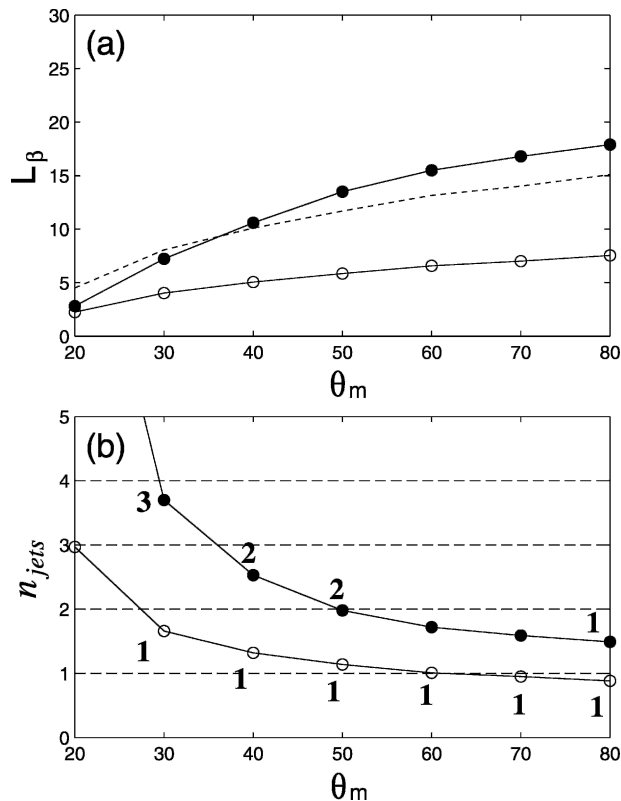


FIG. 6. (a) Rhines scale L_β and (b) estimated n_{jets} . The open circles are for the Earth set and the filled circles are for the large-planet set. The dashed line in (a) is $2 \times L_{\beta, \text{Earth}}(\theta_m)$, where $L_{\beta, \text{Earth}}(\theta_m)$ is L_β of the Earth run. The boldface numbers next to the circles indicate the number of jets simulated in the numerical model. No numerical value is assigned for the cases where the simulated jet number is ambiguous.

set u_{rms} equal to the square root of the total EKE. For the sake of consistency, the latitudinal averaging of $\langle u_{\text{rms}} \rangle$ is now performed with $\phi_S = \phi_\xi$ and $\phi_N = \phi_\xi + 60^\circ$, instead of the standard limits used elsewhere in this study. The result, which is displayed with the dashed line in Fig. 1, is not very different from the averaging based on the standard limits (filled diamonds). When the barotropic EKE density V is used (cf. Held and Larichev 1996), the value of L_β is only slightly smaller (open diamonds), and the result remains essentially the same.

Because noninteger values are not realizable, the integer truncated at the decimal point should be regarded as the jet number. Except for the 20-K cases where the EKE level is very low, these estimates (Fig. 6b) are reasonably close to those simulated by the model (Fig. 2). To help the comparison, the actual simulated jet number, when unambiguous, is also indicated in Fig. 6b. The exceptions are the 80-K case of the Earth set for which the estimated n_{jets} is less than 1, and the 60 and

70-K cases of the large-planet set where the n_{jets} in the numerical model is rather ambiguous.

It is concluded then that (2)–(4) provide a useful guideline as long as the domain is sufficiently large so that L_o^{-1} is not bounded by the domain itself. With this overall picture in hand, the next section examines these multiple jets.

4. Eddy fluxes and maintenance of the multiple jets

With the large-planet set, the extent to which the multiple jets on the sphere are maintained in the same manner as those in the QG model on the β plane (Panetta 1993; Lee 1997) is examined. Because multiple jets are most ubiquitous and persistent for the 30-K case, this run is analyzed in detail. As can be seen from a snapshot of the eddy streamfunction and upper-level potential vorticity fields (Fig. 7), while the signature of the multiple jets is still apparent (see the right panels in Fig. 7), the flow is turbulent and reminiscent of atmospheric flows. The characteristics of the eddy fluxes in this case, as can be seen from the phase-speed spectra of the eddy heat flux and the eddy momentum flux convergence (see Figs. 8a and 8b, respectively), are similar overall to those from the QG model on the β plane [see Fig. 5 of Lee (1997)].

An examination of the poleward heat flux (Fig. 8a) reveals seven local maxima (indicated by filled dots), although the ones at $\approx 70^\circ$ and $\approx 75^\circ$ are barely discernible. Three of these maxima are associated with eastward propagating waves, and are located at each of the three extratropical jet centers (at $\approx 35^\circ$, 55° , and 70°), indicating that wave source for each jet is confined within the same jet. The other four centers occur at the latitudes of local jet minima (at $\approx 30^\circ$, 45° , 60° , and 75°). Also noteworthy is that heat flux maxima in Fig. 8a coincide roughly with lower-level critical latitudes, as can be seen by comparing the heat flux spectra with the lower-level wind speed. Although not discussed, a similar feature can be seen in the QG model [Figs. 4a, 5a, and 7e in Lee (1997)], and also in the observed Southern Hemisphere (SH) flow where the maxima in the 700-hPa poleward heat flux closely follows the mean surface zonal wind [Fig. 3 in Kim and Lee (2004)].⁵

Figure 8b shows that at the jet centers, eastward moving baroclinic waves accelerate the zonal winds. Furthermore, assuming that the zonal phase speed of these waves is conserved as they propagate meridionally, it

⁵ The lower-level flow in a two-level model is dynamically analogous to the surface flow in a continuous model/atmosphere.

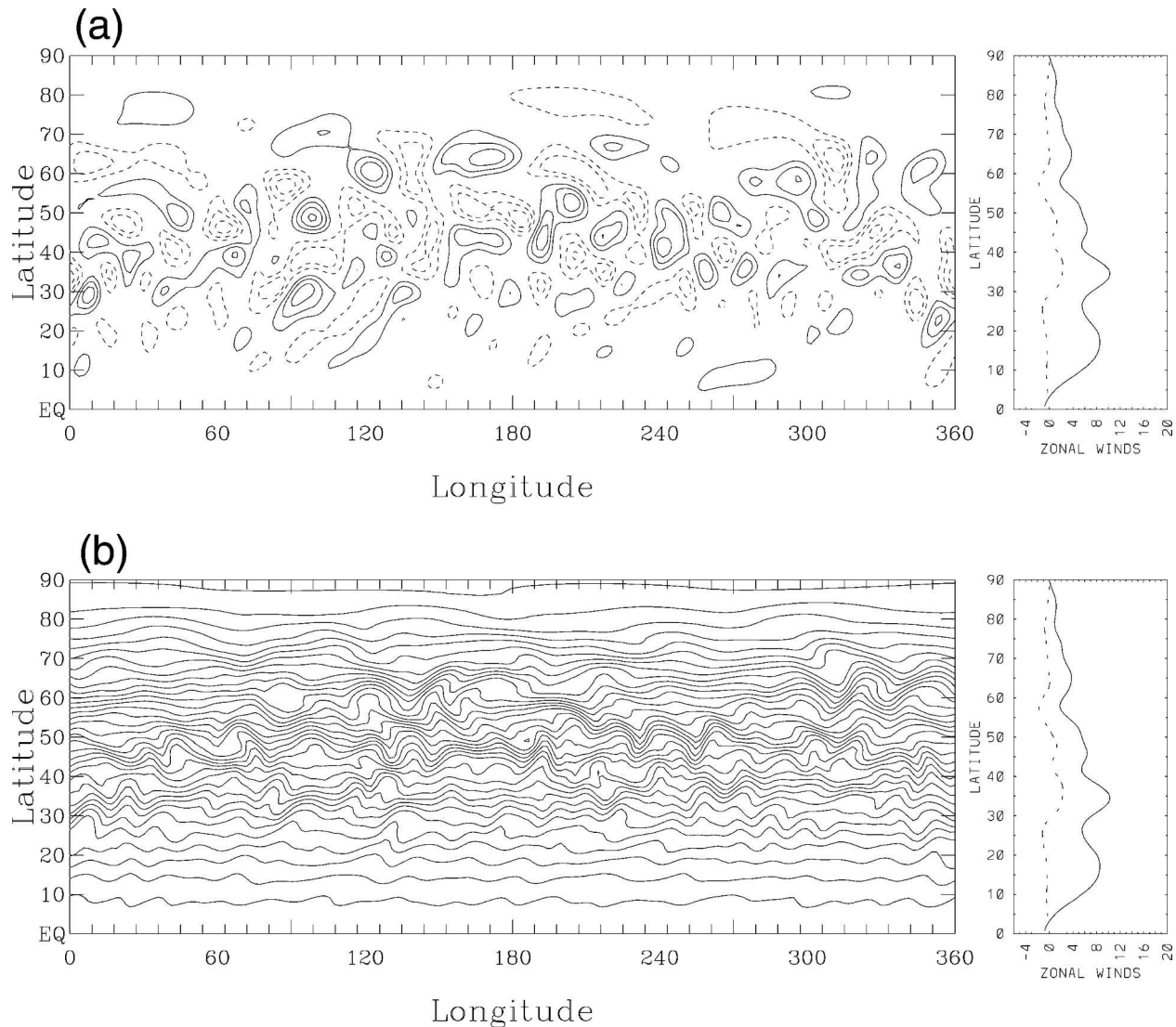


FIG. 7. A snapshot (day 10 in Fig. 6a) of the upper-level (a) eddy streamfunction and (b) quasigeostrophic potential vorticity for the large-planet 30-K case. The contour interval is (a) $5 \times 10^6 \text{ m}^2 \text{ s}^{-1}$ and (b) $2 \times 10^{-5} \text{ s}^{-1}$. (right) The corresponding zonal-mean zonal wind: solid line is for the upper level and dashed line for the lower level.

can also be inferred from Fig. 8b that the same waves are absorbed at the critical latitudes at both sides of the jets. This process keeps the jets from broadening, and thus maintains the identity of the multiple jets.

In addition to the jet-confined, eastward propagating waves, there are also westward propagating, slow baroclinic waves at the extratropical jet minima between the eddy-driven jets [these baroclinic waves are referred to as interjet disturbances in Lee (1997)]. As described above, the associated poleward eddy heat fluxes indicate that these are baroclinic waves, and that their sources are located at each of the local jet minima. These westward propagating waves also contribute toward maintaining the identity of the multiple jets by

decelerating the zonal winds at the local jet minima. Figure 8b shows that momentum flux divergence centers are located at each of the extratropical local jet minima, with the most significant contributions coming from waves whose phase speed is equal to the local zonal wind speed in the lower level. These features are all consistent with the results from the QG channel model (Lee 1997).

There is one exception to the above parallelism between the QG channel model and the PE spherical model. This takes place at the low-latitude jet minimum (near 30°), which borders both the subtropical jet and the southernmost eddy-driven jet. Associated with the local heat flux maximum at this location, the momen-

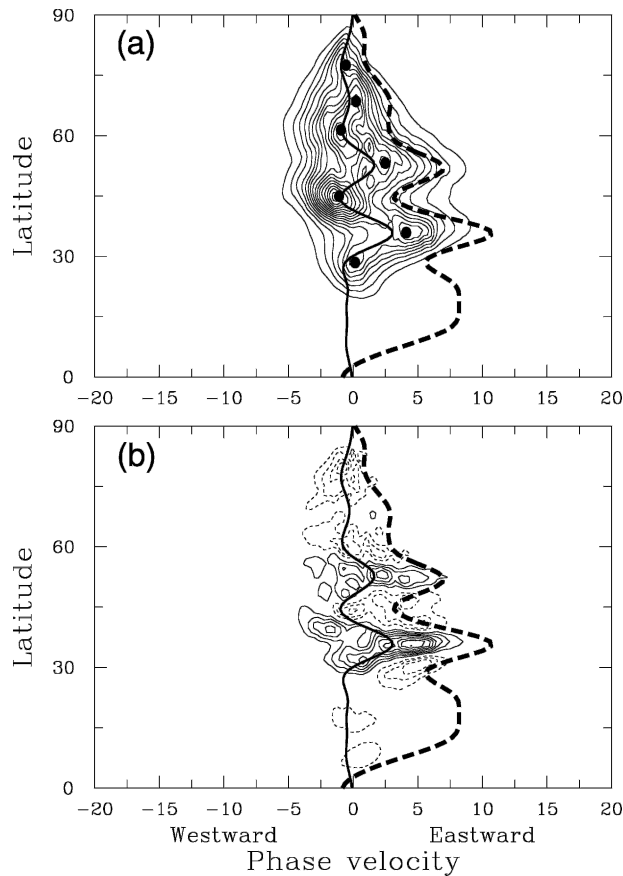


FIG. 8. The power spectral density of (a) the lower-level eddy heat flux and (b) the upper-level eddy vorticity flux for $\theta_m = 30$ K in the large-planet set. The contour interval is $4 \times 10^{-2} \text{ K m s}^{-1} (\Delta c)^{-1}$ for (a) and $8 \times 10^{-8} \text{ m s}^{-2} (\Delta c)^{-1}$ for (b), where $\Delta c = 0.25 \text{ m s}^{-1}$. Superimposed on (a) and (b) with thick lines are the time-mean zonal-mean zonal winds in the upper level (dashed) and in the lower level (solid). The black dots in (a) represent local maxima in the eddy heat flux.

tum flux convergence of the slow waves shows a pronounced latitudinal asymmetry. Unlike for the extratropical jet minima, there is a momentum flux convergence center only to its north. Provided once again that the zonal phase speed of the wave is conserved, Fig. 8b indicates that this momentum flux convergence is compensated by momentum flux divergence on the equatorward side of the subtropical jet. Since this momentum flux divergence accounts for essentially all of the momentum flux divergence in this region, it follows that it is these slow baroclinic waves that dominate the wave-driven zonal wind deceleration in the Tropics/subtropics of this model. This behavior is not only confined to this model, but it also resembles that observed during the SH winter (Kim and Lee 2004), and clearly arises from the spherical geometry which was absent in the QG channel model.

5. Consideration of baroclinic adjustment and diffusivity

In addition to the relationship amongst the planetary size, baroclinicity, and jet number, the two sets of model runs provide useful insight into the relevance of baroclinic adjustment and eddy diffusion parameterizations for the atmosphere. Accordingly, this section examines baroclinic adjustment and eddy diffusivity in the model runs.

We begin the discussion by first considering the following flux–gradient relationship:

$$\overline{v'\chi'} = -D_\chi \frac{\partial \bar{\chi}}{\partial y}, \quad (5)$$

where χ is an arbitrary scalar field, which may be either heat (θ) or potential vorticity, and D_χ is the eddy diffusivity. The overbar denotes an appropriate averaging, such as time mean or zonal mean, and the prime indicates the deviation from the mean. Such flux–gradient relationships are useful if D_χ varies little throughout the midlatitudes. The relevance of this relationship for the multiple jet state can be gleaned from the structure of the eddy heat flux. While the heat flux structure is rather complex in the phase-speed space (Fig. 8a), when contributions from all phase speeds are summed, the resulting meridional profile exhibits a much simpler structure (Fig. 2). This profile resembles the meridional gradient of the time-mean zonally averaged θ (not shown) whose meridional structure is not too different from that for the equilibrium profile [see (1)]. This remains the case for all other simulations that are examined in this study (see the eddy heat flux in Fig. 2).

In the large-planet set, for cases where l_0 is not limited by the domain size ($\theta_m \leq 50$ K), the diffusive picture of Held and Larichev (1996) holds reasonably well. Figure 9b shows the vertically and latitudinally averaged poleward eddy heat flux $\{\langle \overline{v'\theta'} \rangle\}$ and diffusivity $\{\langle D_\theta \rangle\}$, where $\{\cdot\}$ denotes a vertical average. The eddy diffusivity D_θ is calculated locally, using (5), and then averaged both latitudinally and vertically. As described in section 2b, the latitudinal averaging is performed over the latitudes between 22.5° and 67.5° . Recalling that ξ_e increases linearly with θ_m , it can be seen that for $\theta_m < 50$ K, both $\{\langle \overline{v'\theta'} \rangle\}$ and $\{\langle D_\theta \rangle\}$ increase more rapidly with θ_m than does ξ_e ; fitting z with the following function of ξ_e ,

$$\frac{z(\theta_m) - z(20 \text{ K})}{z(50 \text{ K}) - z(20 \text{ K})} = \left[\frac{\xi_e(\theta_m) - \xi_e(20)}{\xi_e(50 \text{ K}) - \xi_e(20 \text{ K})} \right]^\alpha,$$

where z may be either $\{\langle \overline{v'\theta'} \rangle\}$ or $\{\langle D_\theta \rangle\}$, a best fit for α is found to be 2.25 for the heat flux, and 2.0 for D_θ . (See

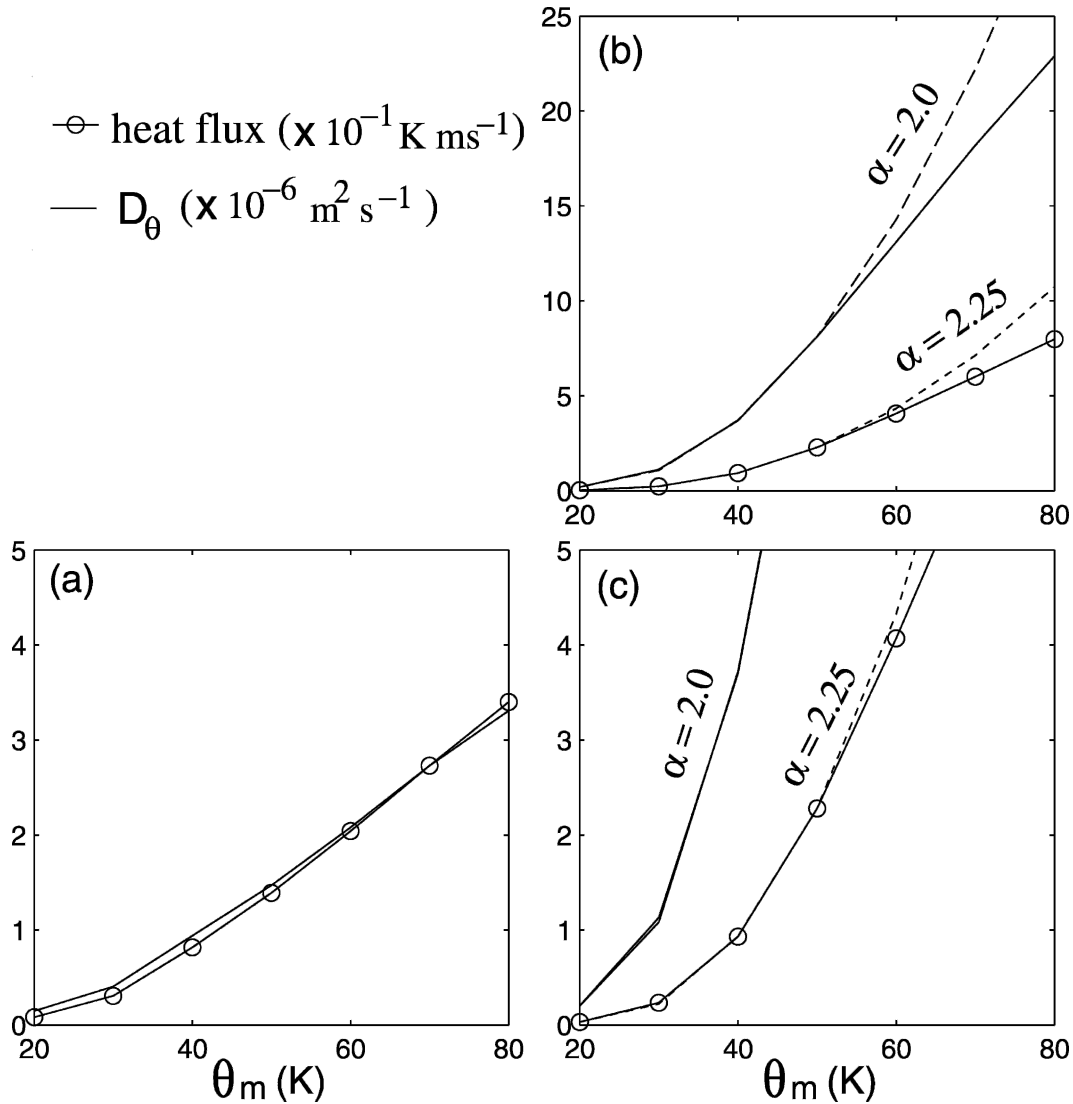


FIG. 9. The lower-level eddy heat flux (open circle) and the corresponding eddy diffusivity (solid line) averaged over latitudes between 22.5° and 67.5° for (a) the Earth and (b) the large-planet set. (c) The bottom 20% of (b), which is shown for a more direct comparison with (a). The short dashed line is the $\alpha = 2.25$ fit for the eddy heat flux, and the long dashed line is the $\alpha = 2$ fit for the eddy diffusivity (see text). The heat flux is scaled by 10 K m s^{-1} and the diffusivity by $10^6 \text{ m}^2 \text{ s}^{-1}$.

the dotted lines in Fig. 9b.) For these values of α , the fit is in good agreement with the model calculations. Also, this value of α is in close agreement with the result of Held and Larichev (1996) who suggest $D \sim U\lambda\xi_c^2$. However, for cases where l_o is limited by domain size (i.e., for $\theta_m \geq 60 \text{ K}$), smaller values of α would lead to a better fit.

In contrast, for the Earth set, baroclinic adjustment seems to be more applicable. With increasing θ_m , the value of the time-mean supercriticality ξ , while not staying near 1.0, as would be the case if baroclinic adjustment were to operate, nevertheless asymptotes to a constant value (Fig. 1a). This result conforms to the

weak baroclinic adjustment picture (Stone and Branscome 1992). The same conclusion can also be drawn based on the behavior of the heat flux and D_θ . Neglecting subgrid-scale diffusion, the zonally and vertically averaged time-mean heat equation for the PE model can be written as

$$\frac{\partial\{\langle\theta\rangle\}}{\partial y} = -\tau \frac{\partial^2}{\partial y^2} \{\langle v'\theta'\rangle\} + \frac{\partial\langle\Theta_e\rangle}{\partial y}, \quad (6)$$

where τ is the radiative relaxation time scale. If weak baroclinic adjustment operates, the lhs of (6) must remain constant. Therefore, any change in the second

term on the rhs, which is proportional to the supercriticality of the radiative equilibrium state $\langle \xi_e \rangle$, must be compensated exactly by the same fractional change in the first term on the rhs. Provided that τ and the length scale for the heat flux are independent of $\langle \xi_e \rangle$, it follows then from (6) that $\{\overline{\langle v'\theta' \rangle}\} \propto \langle \xi_e \rangle$. Except for $20 \text{ K} \leq \theta_m \leq 30 \text{ K}$, this relationship indeed occurs, as can be seen by noting that $\{\overline{\langle v'\theta' \rangle}\}$ is a linear function of θ_m (see Fig. 9a), as is $\langle \xi_e \rangle$ [see (3)].

6. Conclusions

On a hypothetical large planet, a flow forced toward an Earthlike baroclinicity can generate and maintain multiple zonal jets. In a manner similar to that obtained for the QG channel model on the β plane, these jets are driven by momentum flux convergence of fast baroclinic waves. In addition, as in the QG model (Lee 1997), the persistence of the multiple jets arises from both the absorption of these fast baroclinic waves at their critical latitudes, and slow baroclinic waves at the extratropical interjet minima. The eddy momentum flux divergence by these slow baroclinic waves at the interjet minima between the jets is found to be ubiquitous, indicating that the presence of these slow baroclinic waves, referred to as interjet disturbances by Lee (1997), is not just limited to the QG channel model. Also consistent with another QG model study (Panetta 1993), for moderately and strongly unstable flows ($\theta_m \geq 30 \text{ K}$), the number of jets is predicted by the Rhines scale with reasonable accuracy. As such, it is concluded that the overall dynamics of multiple jets in this PE model calculation is consistent with that from the QG β -plane channel model.

Unlike for the QG channel model, however, in this PE model on the sphere, a subtropical jet also forms. For the 30-K case of the large-planet set, a pure subtropical jet coexists with multiple eddy-driven jets, however, as the value of θ_m increases, the subtropical jet starts to blend with adjacent eddy-driven jet. For the Earth set, the eddy-driven and subtropical jets are always blended to form a single jet. This result is consistent with an earlier study by Chen (1994). With a model essentially identical to the one used in this study, he showed for a very weak equilibrium temperature gradient that a subtropical jet separates itself from the eddy-driven jet, forming a double-jet state.⁶ These re-

sults suggest that had the Earth's baroclinic zone been broader and/or the overall baroclinicity been weaker, there would be a clearer separation between the subtropical and eddy-driven jets than is observed (cf. Williams and Holloway 1982; Son and Lee 2005). These results also appear to be relevant for the calculations performed by Williams (1988). In the present study, the eddy vorticity flux structure of the blended jet is reminiscent of the "QG - γ " flow of Williams (1988). On the other hand, his "QG - β " flow strongly resembles the eddy-driven jets here, suggesting that the difference between the QG - γ and the QG - β may stem from the presence or absence of blending with the subtropical jet.

The eddy kinetic energy spectra suggest that the meridional scale of the energy containing eddies in the Earth set is severely limited by the domain size. This is not the case for the large-planet set, as long as the pole-to-equator gradient of equilibrium temperature is not too large (i.e., $\theta_m \leq 50 \text{ K}$) so that the meridional scale of the most energetic eddies remains smaller than the domain size. This is consistent with the result that the baroclinic adjustment picture holds well for the Earth set, but not for the large-planet set. For the latter set, within the range of $20 \text{ K} \leq \theta_m \leq 50 \text{ K}$, the Held and Larichev (1996) scaling for eddy diffusion is found to be valid. The above contrast between the Earth and large-planet sets suggests that the success of baroclinic adjustment (Stone 1978; Stone and Branscome 1992) is not only due to two-layer model dynamics but also to the fact that the baroclinic zone for the Earth-like parameter setting is narrow (cf. Pavan and Held 1996). Considering the fact that two-layer models are more prone to baroclinic adjustment, it seems fair to conclude from this study that Earth's atmosphere is close to being at the boundary between the two regimes—baroclinic adjustment and diffusive. This is also consistent with the finding that the baroclinic adjustment picture fits better for some regions of the atmosphere, but not for others (Stone and Nemet 1996).

While the scaling analysis in section 2 yields a result consistent with the numerical simulations, a question still remains as to what determines the proportionality constant between u_{rms} and ξ_e in (3). This is closely related to the question of what process stops the upscale energy cascade when the planetary size plays no role (cf. Vallis and Maltrud 1993; Held and Larichev 1996), and therefore to the equilibrium process that is only touched upon in this study. An answer to this question calls for both theoretical analyses and a more systematic set of numerical experiments (e.g., consideration of systematically larger planets) than is considered in this study.

⁶ This equilibrium temperature field of Chen (1994) is equivalent to $\theta_m = 9.125 \text{ K}$ of this study. Other notable model specifications that differ from those used here include the value of τ , which is 15 days, and the horizontal resolution, which is an R42.

Acknowledgments. This research was supported by the National Science Foundation through Grant ATM-0324908. The author is grateful to three anonymous reviewers for their helpful comments that led to a significant improvement of this manuscript. In particular, one of the reviewers suggested using the precise form for the equilibrium supercriticality (A5). The same reviewer also suggested that the latitude ϕ_ξ can be used to distinguish the eddy-driven jet from the subtropical jet.

APPENDIX

Derivation of (3)

The supercriticality of the Phillips (1956) two-layer model is defined as

$$\xi \equiv \frac{U}{\beta\lambda^2}, \quad (\text{A1})$$

where U is the vertical shear defined as $(U_1 - U_2)/2$ with U_1 and U_2 being the upper- and lower-level zonal winds, respectively. In the two-layer QG β -plane approximation corresponding to the PE model here, the Rossby deformation radius λ takes the form

$$\lambda = \frac{(BC_p\Delta\theta/2)^{1/2}}{f}, \quad (\text{A2})$$

where $B \equiv [(p_2/p_*)^{R/C_p} - (p_1/p_*)^{R/C_p}]/2$ with $(p_*, p_1, p_2) = (1000, 250, 750)$ hPa, C_p is the heat capacity per unit mass at constant pressure, and R is the gas constant [see Held and Suarez (1978) for a more complete description of the model and the constant B]. Except for the value of B , λ^2 here is identical to $(2\lambda_R^2)^{-1}$ in Saravanan (1993).

The thermal wind relation in the PE model is

$$U = -\frac{BC_p}{f} \frac{\partial \bar{\theta}}{a \partial \phi}. \quad (\text{A3})$$

With the help of (A2) and (A3), (A1) can be rewritten as

$$\xi = \frac{-\partial \bar{\theta} / \partial \phi}{(a\beta\Delta\theta)/2f}. \quad (\text{A4})$$

By setting $\bar{\theta} = \Theta_e$ given by (1), the supercriticality of our radiative equilibrium state takes the form of

$$\xi_e = 8 \sin^2 \phi \frac{\theta_m}{\Delta\theta}. \quad (\text{A5})$$

REFERENCES

- Baer, F., 1972: An alternative scale representation of atmospheric energy spectra. *J. Atmos. Sci.*, **29**, 649–664.
- Barry, L., G. C. Craig, and J. Thurn, 2000: A GCM investigation into the nature of baroclinic adjustment. *J. Atmos. Sci.*, **57**, 1141–1155.
- Cehelsky, P., and K. K. Tung, 1991: Nonlinear baroclinic adjustment. *J. Atmos. Sci.*, **48**, 1930–1947.
- Chen, B., 1994: Double jets and storm tracks in a two-level primitive equation model of the atmosphere. Ph.D. thesis, Texas A&M University, 131 pp.
- Charney, J. G., and M. E. Stern, 1962: On the stability of internal baroclinic jets in a rotating atmosphere. *J. Atmos. Sci.*, **19**, 159–172.
- Cho, J. Y.-K., and L. M. Polvani, 1996: The emergence of jets and vortices in freely evolving, shallow-water turbulence on a sphere. *Phys. Fluids*, **8**, 1531–1552.
- Ellsaesser, H. W., 1966: Evaluation of spectral versus grid methods of hemispheric numerical weather prediction. *J. Appl. Meteor.*, **5**, 246–262.
- Gutowski, W. J., Jr., 1985: Baroclinic adjustment and midlatitude temperature profiles. *J. Atmos. Sci.*, **42**, 1733–1745.
- Held, I. M., 1999: The macroturbulence of the troposphere. *Tellus*, **51A–B**, 59–70.
- , and M. J. Suarez, 1978: A two-level primitive equation atmospheric model designed for climatic sensitivity experiments. *J. Atmos. Sci.*, **35**, 206–229.
- , and V. D. Larichev, 1996: A scaling theory for horizontally homogeneous, baroclinically unstable flow on a beta-plane. *J. Atmos. Sci.*, **53**, 945–952.
- Hendon, H. H., and D. L. Hartmann, 1985: Variability in a nonlinear model of atmosphere with zonally symmetric forcing. *J. Atmos. Sci.*, **42**, 2783–2797.
- Huang, H. P., and W. A. Robinson, 1998: Two-dimensional turbulence and persistent zonal jets in a global barotropic model. *J. Atmos. Sci.*, **55**, 611–632.
- , B. Galperin, and S. Sukoriansky, 2001: Anisotropic spectra in a two-dimensional turbulence on the surface of a rotating sphere. *Phys. Fluids*, **13**, 225–240.
- Kim, H.-K., and S. Lee, 2004: The wave-zonal mean flow interaction in the Southern Hemisphere. *J. Atmos. Sci.*, **61**, 1055–1067.
- Krishnamurti, T. N., 1961: The subtropical jet stream of winter. *J. Meteor.*, **18**, 172–191.
- Lee, S., 1997: Maintenance of multiple jets in a baroclinic flow. *J. Atmos. Sci.*, **54**, 1726–1738.
- , and I. M. Held, 1993: Baroclinic wave packets in models and observations. *J. Atmos. Sci.*, **50**, 1413–1428.
- , and H.-K. Kim, 2003: The dynamical relationship between subtropical and eddy-driven jets. *J. Atmos. Sci.*, **60**, 1490–1503.
- Lindzen, R., 1993: Baroclinic neutrality and the tropopause. *J. Atmos. Sci.*, **50**, 1148–1151.
- , B. Farrell, and K.-K. Tung, 1980: The concept of wave over-reflection and its application to baroclinic instability. *J. Atmos. Sci.*, **37**, 44–63.
- Nakamura, N., 1999: Baroclinic–barotropic adjustments in a meridionally wide domain. *J. Atmos. Sci.*, **56**, 2246–2260.
- Palmén, E., and C. W. Newton, 1969: *Atmospheric Circulation Systems*. International Geophysics Series, Vol. 13, Academic Press, 603 pp.
- Panetta, R. L., 1993: Zonal jets in wide baroclinically unstable regions: Persistence and scale selection. *J. Atmos. Sci.*, **50**, 2073–2106.
- , and I. M. Held, 1988: Baroclinic eddy fluxes in a one-dimensional model of quasi-geostrophic turbulence. *J. Atmos. Sci.*, **45**, 3354–3365.

- Pavan, V., and I. M. Held, 1996: The diffusive approximation for eddy fluxes in baroclinically unstable jets. *J. Atmos. Sci.*, **53**, 1262–1272.
- Phillips, N. A., 1956: The general circulation of the atmosphere: A numerical experiment. *Quart. J. Roy. Meteor. Soc.*, **82**, 123–164.
- Platzman, G. W., 1960: The spectral form of the vorticity equation. *J. Atmos. Sci.*, **17**, 635–644.
- Rhines, P. B., 1975: Waves and turbulence on a β -plane. *J. Fluid Mech.*, **69**, 417–443.
- , 1977: The dynamics of unsteady currents. *The Sea*, E. D. Goldberg et al., Eds., Marine Modeling, Vol. 6, Wiley and Sons, 189–318.
- Saravanan, R., 1993: Equatorial superrotation and maintenance of the general circulation in two-level models. *J. Atmos. Sci.*, **50**, 1211–1227.
- Son, S.-W., and S. Lee, 2005: The response of westerly jets to thermal driving in a primitive equation model. *J. Atmos. Sci.*, in press.
- Stone, P. H., 1978: Baroclinic adjustment. *J. Atmos. Sci.*, **35**, 561–571.
- , and L. Branscome, 1992: Diabatically forced, nearly inviscid eddy regimes. *J. Atmos. Sci.*, **49**, 355–368.
- , and B. Nemet, 1996: Baroclinic adjustment: A comparison between theory, observations, and models. *J. Atmos. Sci.*, **53**, 1663–1674.
- Thuburn, J., and G. C. Craig, 1997: GCM tests of theories for the height of the tropopause. *J. Atmos. Sci.*, **54**, 869–882.
- Vallis, G. K., and M. E. Maltrud, 1993: Generation of mean flows and jets on a beta plane and over topography. *J. Phys. Oceanogr.*, **23**, 1346–1362.
- Whitaker, J. S., and C. Snyder, 1993: The effects of spherical geometry on the evolution of baroclinic waves. *J. Atmos. Sci.*, **50**, 597–612.
- Williams, G. P., 1978: Planetary circulations: 1. Barotropic representation of Jovian and terrestrial turbulence. *J. Atmos. Sci.*, **35**, 1399–1426.
- , 1979: Planetary circulations: 2. The Jovian quasi-geostrophic regime. *J. Atmos. Sci.*, **36**, 932–968.
- , 1988: The dynamical range of global circulations—I. *Climate Dyn.*, **2**, 205–260.
- , 2003: Jovian dynamics. Part III: Multiple, migrating, and equatorial jets. *J. Atmos. Sci.*, **60**, 1270–1296.
- , and J. L. Holloway, 1982: The range and unity of planetary circulations. *Nature*, **297**, 295–299.
- Yoden, S., and M. Yamada, 1993: A numerical experiment on two-dimensional decaying turbulence on a rotating sphere. *J. Atmos. Sci.*, **50**, 631–643.